

# Corrosion Characterization Using Micro-CT 3D Reconstruction

Nicholas Peterson

(Dated: November 17, 2025)

Monofrax® K-3, an electro-fused chromium alumina refractory material, serves as the primary lining refractory of the joule-heated ceramic melters for the Hanford nuclear waste vitrification effort. While K-3 is highly corrosion resistant, the corrosion damage of the K-3 melter lining refractory caused by the molten glass at the melt line is one of the critical factors limiting the melter life. Thus, characterization of this corrosion behavior is critical in optimizing waste glass compositions and to predict operational downtime. To evaluate the corrosion behavior as a function of glass melt composition, temperature, and test duration, a laboratory-scale bubbled crucible melt test methodology was developed and utilized. Following the termination of the test, the K-3 refractory corrosion depth was then evaluated. This study compares two methodologies for acquiring and analyzing corrosion depth data. Both traditional cross-section analysis with optical microscopy and a micro-computed tomography (micro-CT) approach from which a 3D model of the test coupon is reconstructed were performed on a set of 18 corroded coupons. Results show that in the case of bubbled crucible melt tests where the K-3 corrosion is asymmetric, micro-CT can capture the unique corrosion behavior with a higher level of sensitivity than the traditional cross-section analysis.

## I. INTRODUCTION

Storage of nuclear waste poses inherent difficulties such as environmental concerns, national security concerns, and the cost associated with long term containment of volatile waste. Vitrification is a process in which glass forming chemicals (GFC) are combined with waste and heated, ultimately melting and immobilizing the hazardous waste chemicals within a chemically durable glass matrix for long term storage [1]. Joule Heated Ceramic Melters, the melter technology used at the Hanford Site, utilize resistive heating, passing a current through the glass itself, effectively self-heating. The melters are lined with Monofrax® K-3, an electro-fused chromium alumina refractory material known for its high corrosion resistance.

Characterization of K-3 corrosion has historically been performed using laboratory-scale crucible tests, which consist of simulating the melter conditions in a laboratory scale furnace [4]. The inclusion of a bubbler, which pumps air into the crucible to simulate the large-scale bubblers which will be present in the Hanford Site melters [1]. The most important result of these lab-scale crucible tests is the corrosion depth that occurs at the melt line, as this is where maximum corrosion will occur [ref number]. Using this measurement and the duration of the experiment, an estimated corrosion rate is obtained, which will be used for modeling purposes.

To measure corrosion depth, ASTM standard C621-09 [2] has historically been used [3]. In this method, corrosion depth is analyzed optically. The test coupon is mounted in epoxy and bisected, then the surface is prepared for optical microscopy. The minimum width of the cross section of both halves is recorded, as is a similar measurement 10mm from the submerged end of the coupon. A novel method utilizes micro computed tomography scanning to measure corrosion depth via three dimensional reconstruction. This work aims to investigate variation between the two methodologies, and compare quantitative results generated from a baseline set of K-3 coupons.

## II. METHODS

Eighteen K-3 coupons were selected for this study.

Glass ID	Type (H/LAW)	Test Condition
LORPM14R1	Low Activity Waste	1100C-1Day, 1150C-1Day, 1150C-3Day, 1150C-6Day, 1200C 1-Day
ORLEC9	Low Activity Waste	1150C-3Day, 1150C-6Day, 1200C-1Day
ORLEC33	Low Activity Waste	1150C-3Day, 1150C-6Day
ORLEC52	Low Activity Waste	1150C-3Day, 1150C-6Day
ORPLA14	Low Activity Waste	1150C-3Day, 1150C-6Day
Al-19	High Level Waste	1150C-3Day, 1150C-6Day
IDMS-ref	High Level Waste	1150C-3Day, 1150C-6Day

FIG. 1. 18 K-3 Coupons used in experiment.

### A. X-ray Diffraction Phase Analysis

The XRD phase analysis consisted of a 2 primary trials, and initial, pure K-3 sample and a cerianite-doped K-3 sample for quantitative phase analysis. cerianite ( $CeO_2$ ) chosen as the reference standard based on its dissimilar peaks to the K-3 sample. 1.5g of K-3 was milled in a tungsten carbide chamber for 2 minutes, and subsequently doped with 0.08g of 51.3 % crystalline  $CeO_2$  (Alfa Aesar). Quantitative analysis was performed on the spiked sample, yielding relative phase compositions.

### B. Refractory Corrosion Test

Coupon corrosion is performed in laboratory scale crucibles as shown in Figure [x]. The crucible setup consists of a ceramic shell, a platinum lining, and ceramic crucible lid (RESCORTM CER- CAST CERAMIC 780, Cotronics Corp., Brooklyn, NY, USA). Within the crucible lid the K-3 coupon is embedded, as is a 3mm diameter platinum bubbling apparatus. The bubbling apparatus is spaced 5mm from the coupon, and the tip is oriented to direct the flow of bubbles towards the coupon. The coupon is cut to a square 1cm profile and to 10cm in length. To ensure stability of the coupon during operation, high-temperature cement is used to secure the K-3 coupon to the lid of the crucible and is set at a 90°angle

to the surface of the crucible lid. Additionally, the coupon is vertically positioned such that there is roughly 5mm of space between the bottom of the crucible and the coupon, accomplished using a removable spacer. After the lid-coupon apparatus has been cemented and cured, 130g of test glass is added to the crucible. This weight is experimentally determined to result in a glass melt depth of 25-30mm, the target range for this experiment. Given the coupon's vertical position and the glass melt depth, the bottom 20mm of the coupon will be submerged.

The temperature of the furnace [insert make model manufacturer] was equilibrated at the appropriate temperature for the test (see test matrix) and the crucible was loaded into the furnace. The furnace was held at a constant temperature according to the time defined by the test matrix and removed with minimal ( $< 15\text{min}$ ) variation.

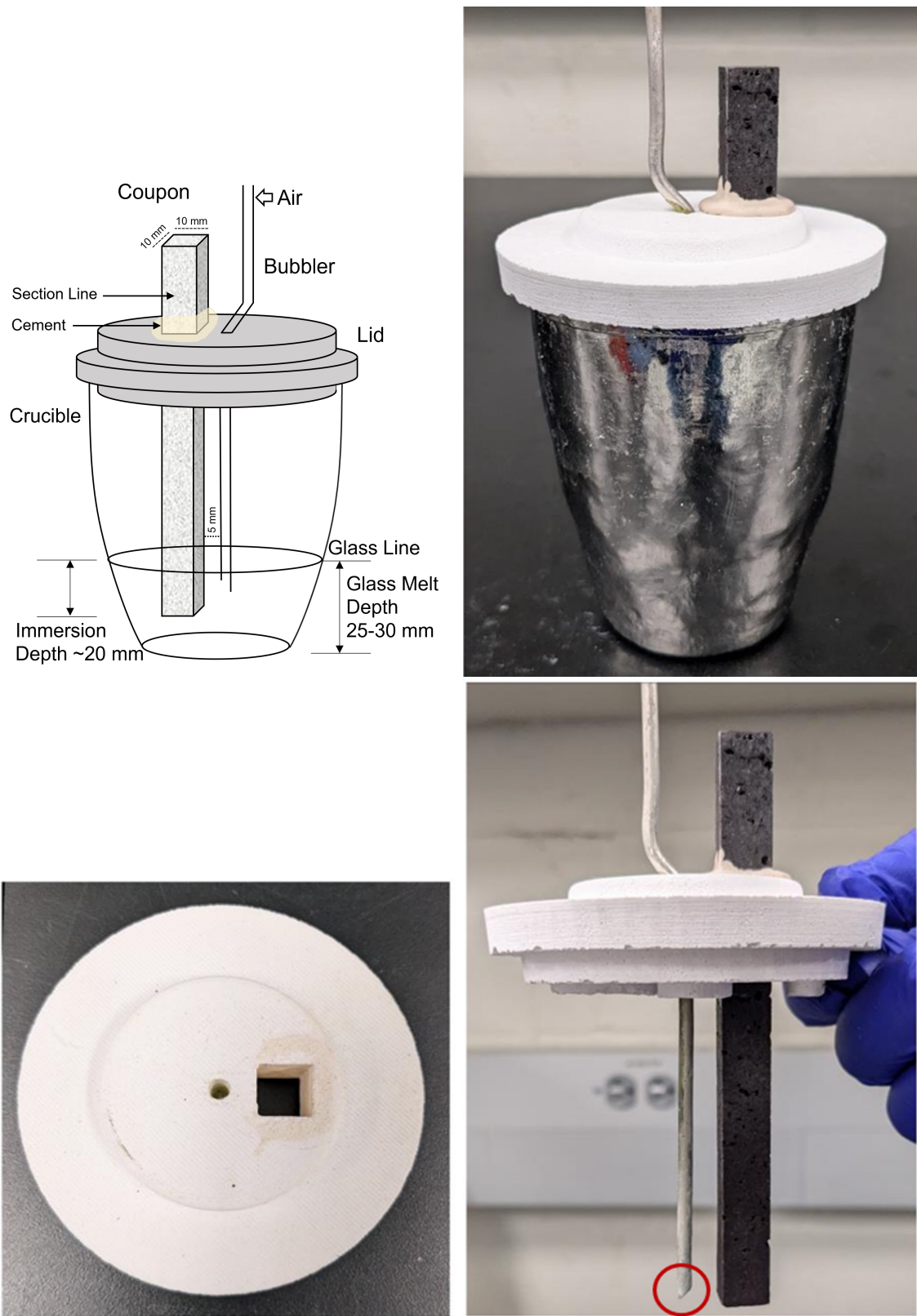


FIG. 2. (Top Left) Schematic of crucible corrosion test experimental setup. (Top Right) Image of model crucible. Ceramic shell not pictured. (Bottom Left) Top-down view of crucible lid. (Bottom Right) Side view of crucible lid with bubbler and coupon inserted.[3]

### C. Corrosion Characterization

#### C1. Optical Characterization

The corrosion of the K-3 Coupons was characterized using micro-computed tomography (micro-CT) and an optical microscopy-based measurement method following ASTM standard C621.

For optical imaging, the post-test K-3 coupons were bisected vertically and mounted in epoxy, followed by polishing and surface preparation. The bisected coupon allows for measurement of both the bubbled and non-bubbled sides, capturing the inherent asymmetry of the corrosion in this work due to the bubbler. The microscopy was performed on a Keyence VH25T at 20x magnification, under mixed conical-ring lighting to minimize glare on the reflective ceramic surface.

The measurements were performed according to an adjusted ASTM C621 standard. The adjustments, made specifically for this procedure, were designed to account for the asymmetry of the corrosion depth on the bubbled and non-bubbled sides. ASTM C621 relies on symmetric corrosion across the width of the coupon, consequently measuring corrosion depth as the minimum width across the entire length of the coupon, as seen in Figure [x]. In the adjusted method, a centerline is over-layed over the coupon and used as the basis for corrosion measurements, allowing for two independent measurements on either side of the coupon.

The micro-CT measurements were performed using a Zeiss Xradia Versa 610 (Carl Zeiss Microscopy GmbH, Jena, Germany) at 150kV, 23W, 0.5s exposure and 2401 projections. The voxel size was  $40\mu m$ . The scans were saved as 2 dimensional cross sections spanning the physical length of the scan. The resultant image stacks were processed using computational image processing software FIJI and Python via PyVista and OpenCV as discussed in depth in the following sections.

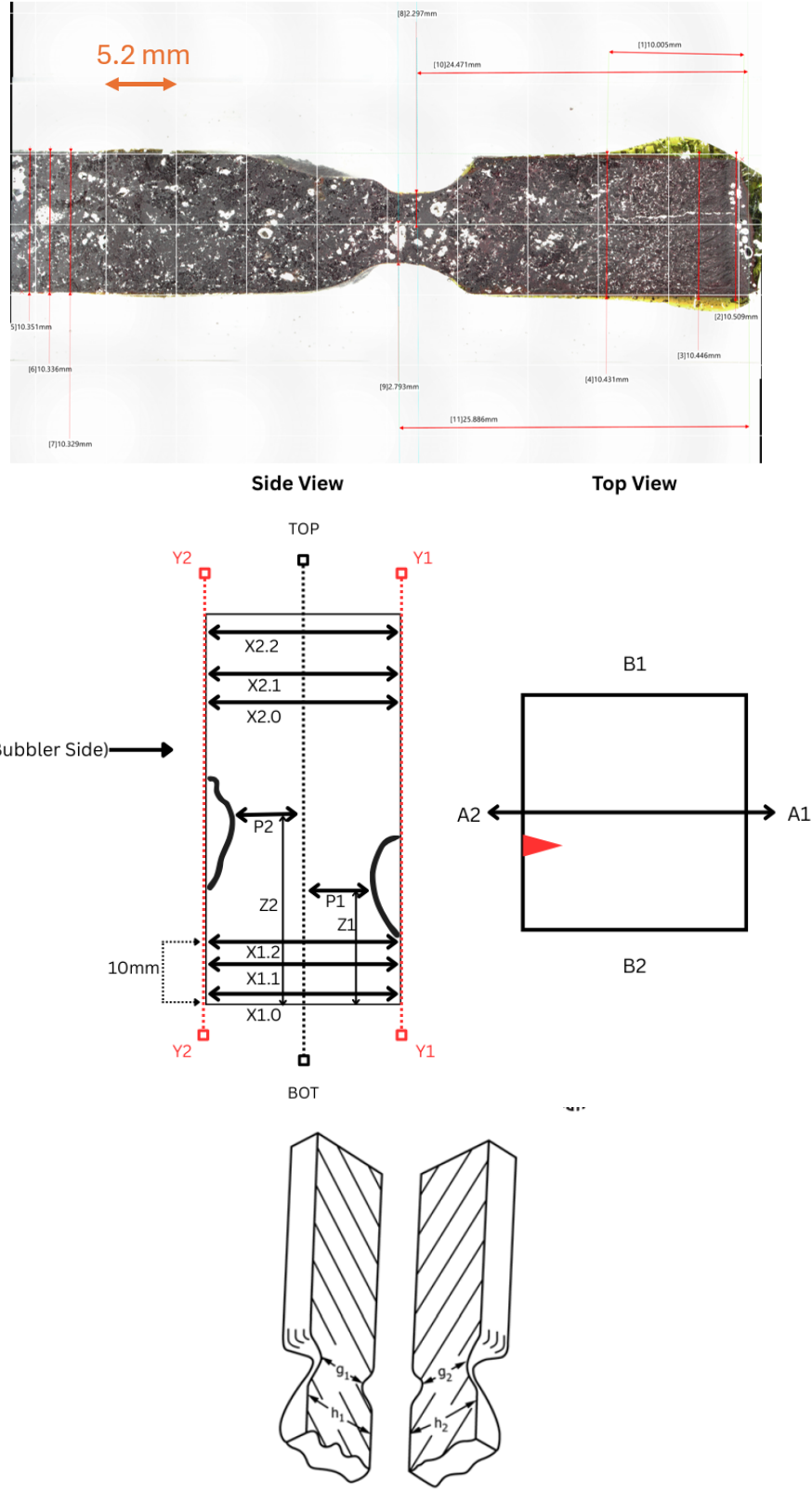


FIG. 2 View of Cut Specimen to Indicate Measurement After Test

FIG. 3. (Top) Optical image of a bisected K-3 Coupon. Grid lines are aligned to act as centerline of the coupon. As seen in (Middle) the corrosion neck depths are denoted P1 and P2. The variation in neck position as seen by Z1 and Z2 validates the necessity of the adjusted ASTM C621 standard. ASTM C621 graphic shown (Bottom)[2].

## C2. Micro-CT Characterization

Processing of the micro-CT scans leverages both pre-treatment and post-treatment scans of the coupon, fundamentally measuring the corrosion depth as a displacement along the  $XY$  plane between the two scans.

Prior to processing the scan takes the form of a stack of 2D images. As mentioned earlier, the scan had a voxel height of  $40\mu m$ , meaning each slice possess the same physical height, which is able to be converted between pixel and physical domains. The first processing stage is to vertically align the slices. An algorithm developed for this purpose uses vector-based geometry to perform a series of rotations, correcting an angle of tilt between the coupon and coordinate axes. The angle of tilt of the z-axis was quantified using the centroids of the top and bottom slices of the reconstructed coupon stack. Mathematically, this was calculated as  $\arctan(dy, dx)$ , where  $dx$  and  $dy$  represent the differences in x and y coordinates, respectively, between the centroids of the top and bottom slices. This calculation determined the angle between the x-axis and the vector connecting the two centroids, thereby defining the degree of lateral ( $x, y$ ) tilt along the z-axis.

To correct this tilt, an iterative rotation and alignment process was performed. First, the top and bottom slice images were rotated on the z-axis to align their centroids along the x-axis. Subsequently, a rotation around the y-axis was applied to correct for the tilt in three-dimensional space. Finally, the stack was rotated back on the z-axis to restore it to its original orientation.

Following this alignment, the centroids of all individual slices were recalculated and averaged. Using this average centroid as the reference point, a  $300 \times 300$  square region of interest was cropped from each slice, ensuring consistent framing across the stack.

The aligned image stack then undergoes thresholding, to segment the K-3 coupon region of the image from the surrounding glass that may be left as a remnant of submersion.

Voids in the coupon present as holes in the image. To correct this, a binary 'fill holes' operation is used. Finally, each image slice is converted to a binary outline, representing only the outermost edge of the coupon.

Next, an algorithm generates bounding boxes surrounding the outline of each slice. This bounding box represents the minimum width of the coupon. These values are converted to  $XY$  coordinates and exported, from which a simple sorting process can identify the maximum difference between the pre-treatment and post-treatment coordinates.

$$depth_{corr,bbl}(z) = X_{bbl}(z) - x_{bbl}(z) \quad (1)$$

$$depth_{corr,far}(z) = X_{far}(z) - x_{far}(z) \quad (2)$$

Where  $X$  and  $x$  represent bounding box width before and after treatment, and  $z$  represents the slice index. Depth corresponds to depth of corrosion, and  $bbl$ ,  $far$ , refer to the specific side of the coupon evaluated. Max corrosion depth is given by:

$$\max(depth) = \max(X(z) - x(z)) \quad (3)$$

Using computational image processing Python libraries OpenCV and PyVista a 3 dimensional and interactive model of the coupon can be generated. Using the Marching Cubes algorithm packaged in PyVista, a contour mesh of the image stack is generated. This mesh is then rendered and can be exported in various graphical design software, such as Blender3D, for enhanced visualization applications.

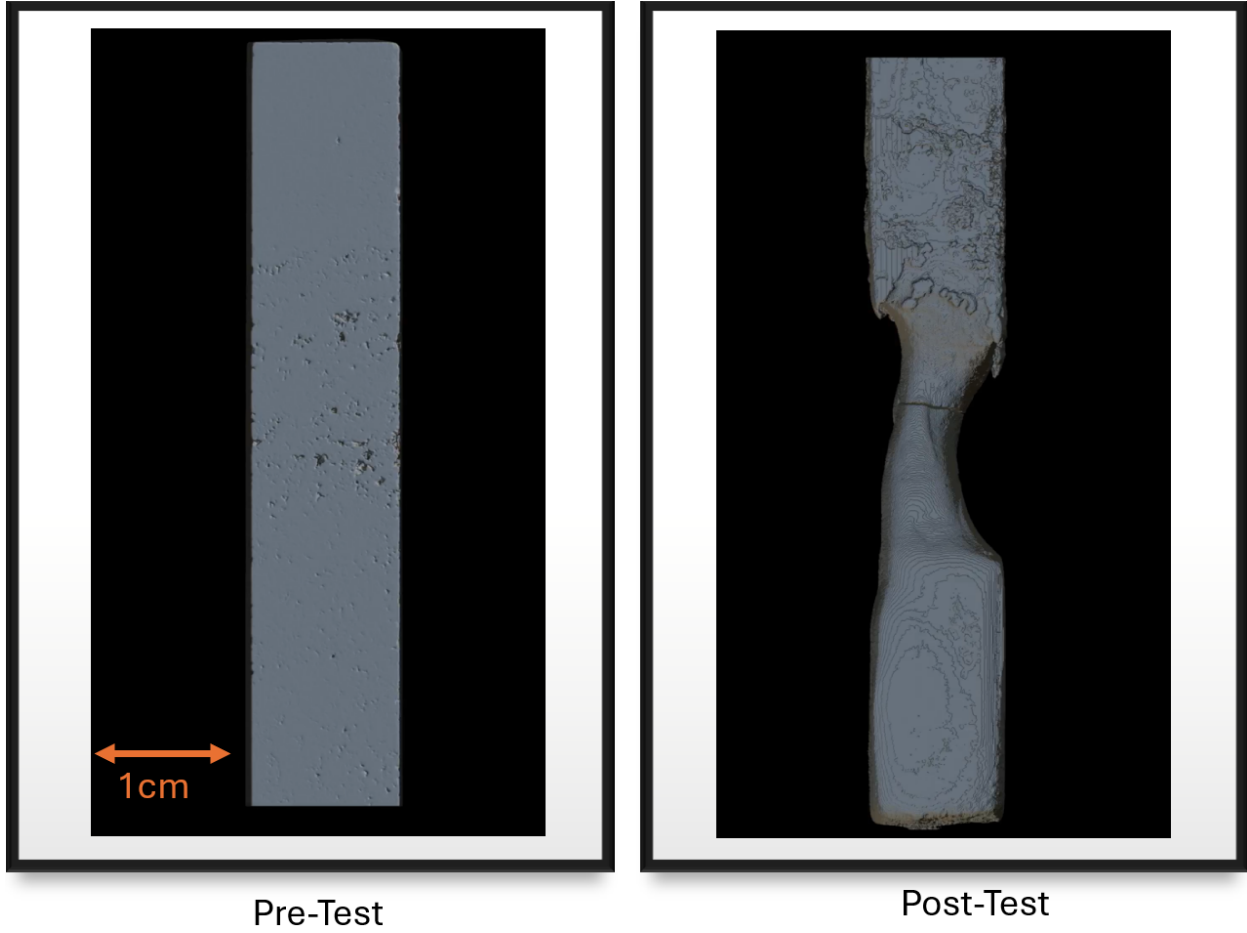


FIG. 4. PyVista generated rendering of pre and post test coupons. Surface modeling is done in Blender3D.

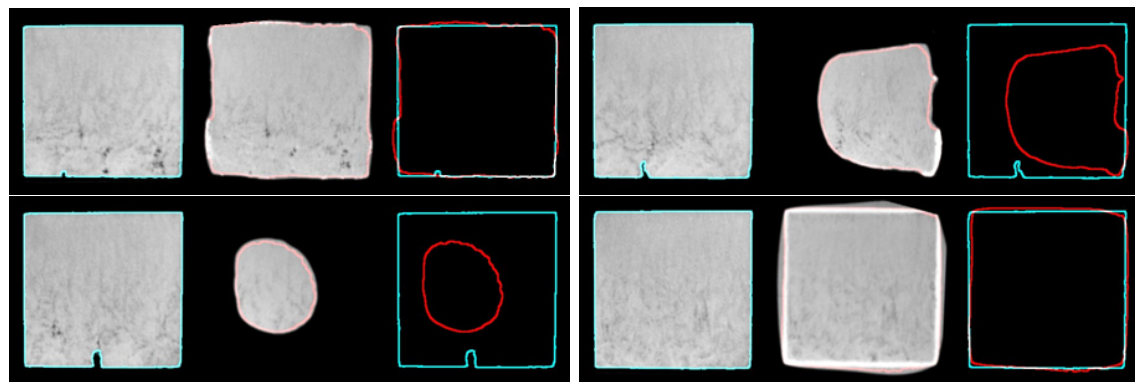


FIG. 5. From left to right (all images) 1. Pre scan slice 2. Post scan slice 3. Pre (blue) and post (red) scan slice outlines overlapped.  
Top Left: Taken at above melt line. Top Right: Higher neck. Bottom Left: Lower neck. Bottom Right: 10mm from bottom.

### III. RESULTS

The main objective of this work was to analytically compare the optical and micro-CT methodologies. This was accomplished via a comparison of the detected neck depth across the evaluated coupons. Across the eighteen coupons evaluated, nine showed nontrivial corrosion. These twelve consist predominantly of test conditions at the higher end of the spectrum, typically 1200°C or 1150°C and test durations of three or six days. While the micro-CT method produced a neck depth for each coupon, the optical imaging method did not.

Across the nine viable coupons, there was mean absolute percentage difference of 48.3% which corresponds to a physical mean absolute difference of  $0.466\text{mm}$ . The largest variation in the data set was 172.9% and the minimum was 1.1%.

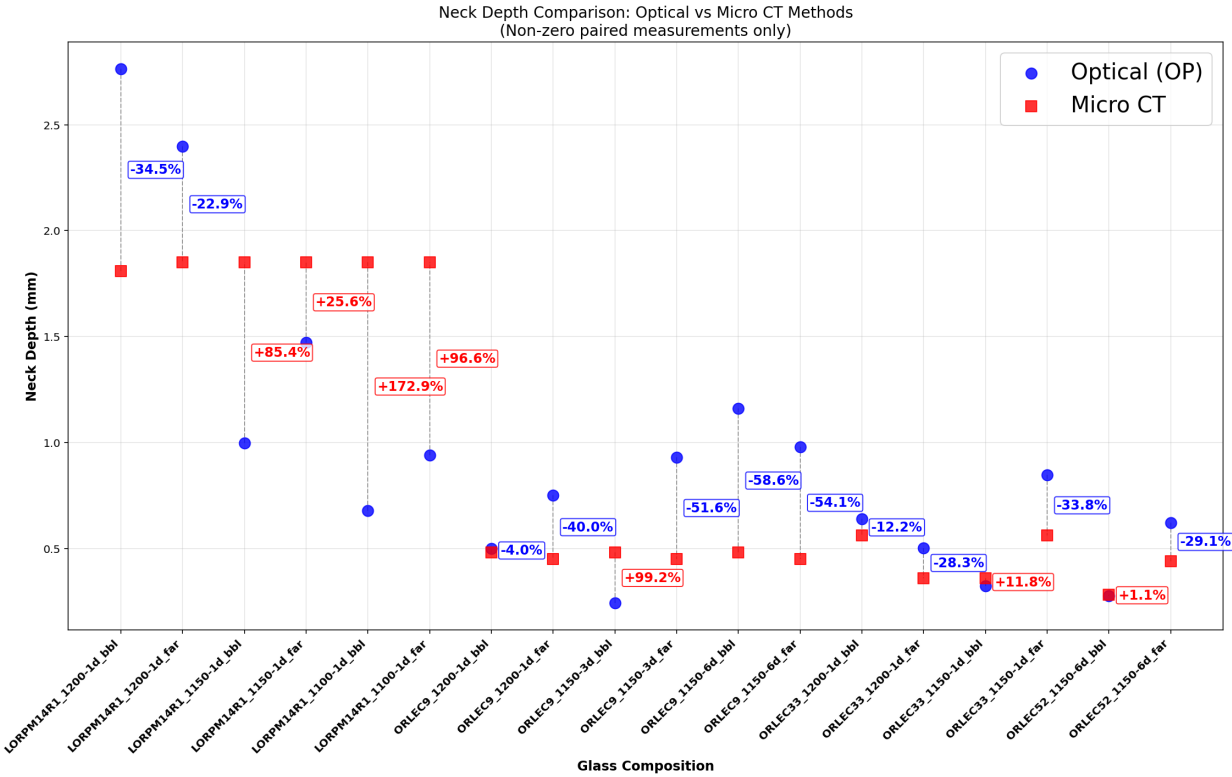


FIG. 6. Plotted optical and micro-CT generated corrosion neck depths. The optical data points are in blue, and the micro-CT in red. Each two successive columns represent the individual sides (bubbler facing and far side) of the bisected K-3 coupon. Variation between data points is shown as a percentage difference.

The quantitative analysis of the cerianite K-3 sample yielded the following compositions:

Phase Name	Wt% Rietveld	Wt% of Spiked ( $S_i$ )	Wt% in Spiked sample ( $X_{sp}$ )	Wt% in Original sample	Normalized Wt% in Original sample (Corrected for Amorphous Content of STD Zincite) ( $N_{wt\%}$ )
Cerianite	4.194	5	5	0	0
Fe0.25Al1.75O <sub>3</sub> (Corundum)	61.001	0	72.716	76.543	39.251
Spinel(Mg,Cr,Fe,Al)	33.45	0	39.874	41.973	21.523
MgAl <sub>2</sub> O <sub>4</sub> -Spinel	1.354	0	1.614	1.699	0.871
Amorphous	-	-	-	-	38.355

FIG. 7. Summarized Quantitative XRD Results.

#### IV. DISCUSSION

Further analysis of the results included a comparison of the vertical position of the neck. This served as secondary confirmation of whether the two approaches had identified the same physical location as the point of maximum corrosion depth. This was done by conversion of a "slice" number at which the maximum neck depth occurred to its corresponding length. This value was compared to the neck position ( $Z_1$  and  $Z_2$ ) in the optical measurements. Significant variations were found in multiple coupons, particularly those that showed relatively large neck depth discrepancies.

This difference in neck position identification can be attributed to the optical methods limitation of a discrete planar measurement, while the micro-CT process can detect and measure corrosion necking through the entire volume of the coupon. Due to the bisection of the coupon and the top-down imaging utilized in optical microscopy, only corrosion occurring specifically along the plane of bisection can be reliably measured.

This results in misidentification of the true neck position, as maximum corrosion may occur elsewhere than the plane of bisection. This discrepancy is illustrated in the figure below.

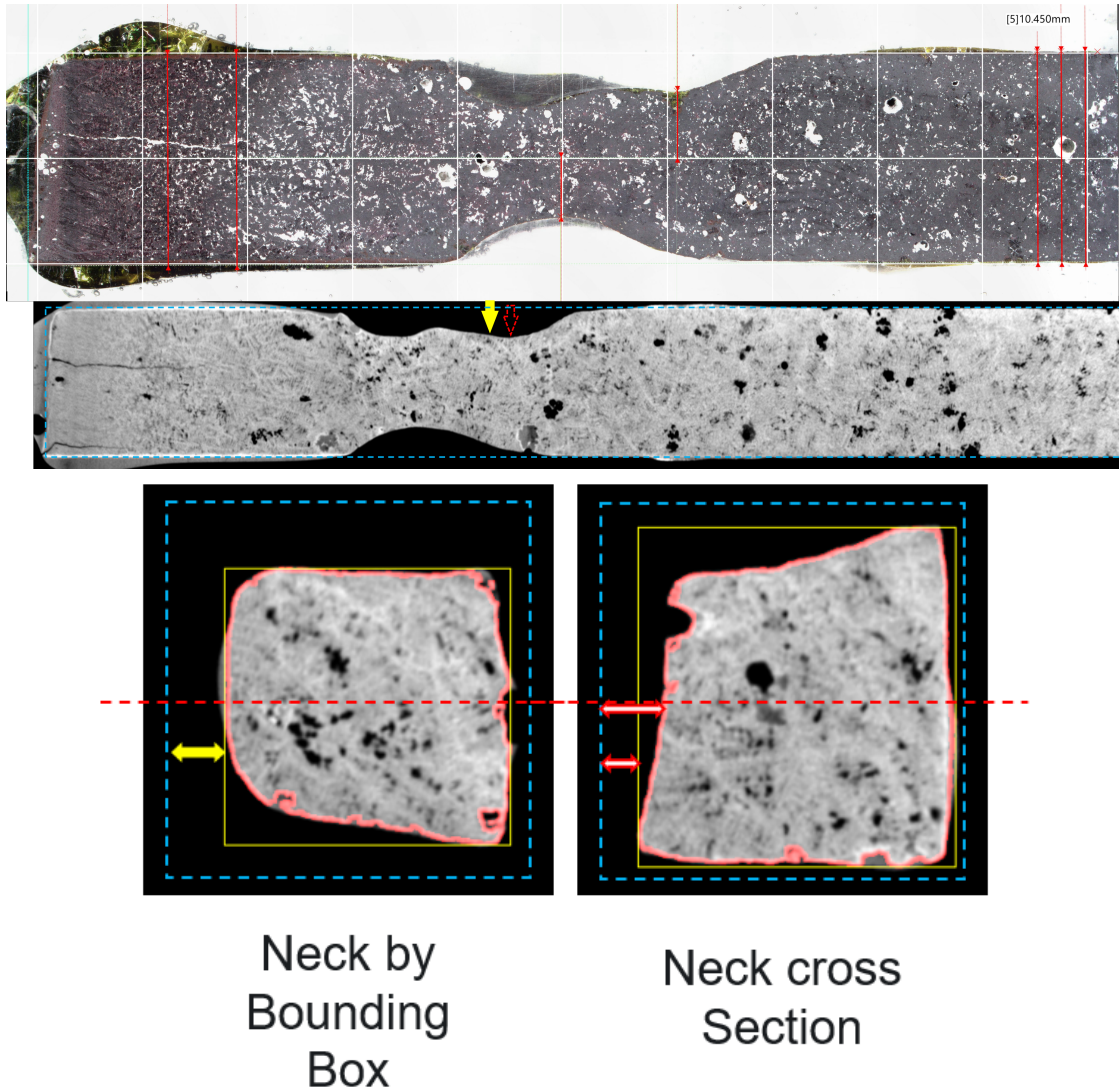


FIG. 8. (Top) Bisected test coupon and equivalent position viewed in micro-CT scan. (Bottom) Cross sections shown at neck positions as informed by both optical and micro-CT methods.

In the above, the red arrow represents the maximum corrosion depth as recorded via the optical method. The image slice shown is taken from the middle of the coupon, an equivalent position to the bisected coupons surface plane. As seen in both the optical and micro-CT image, this appears to be the maximum depth. However, using the bounding box approach, the point of maximum corrosion is further down, shown by the yellow arrow. This point is not visible using the optical method as it is above the plane of bisection. As seen by the bounding box illustrations, the variation in locating the neck position between methods

leads to significant error in neck depth measurements.

In the case of bubbled, asymmetric coupon corrosion testing as discussed in this work, optical microscopy-based characterization poses significant challenges primarily due to the physical limitation of the bisection procedure. Micro-CT based characterization is well equipped to handle this asymmetry, and provides other benefits such as a decreased processing time, non-destructive evaluation, and 3-dimensional replication. In future evaluation, static (non-bubbled) coupon corrosion results will be compared to establish a baseline error between the two methodologies, when obstructing factors such as asymmetry are not present.

#### ACKNOWLEDGMENTS

Thank you to the MSIPP-EM internship program for graciously funding this work, as well as the members of the Radiological Materials Group at PNNL. Specifically, Tongan Jin (Mentor), Nathan Canfield (Micro-CT operator), Emily Nienhuis-Marcial (Mentor) and Mark Hall (Project Manager). Additionally, thank you the MSIPP coordinator Sabrina Hoyle for managing my internship process.

- 
- [1] J. Marcial, B. J. Riley, A. A. Kruger, C. E. Lonergan, and J. D. Vienna, Journal of Hazardous Materials 461, 132437 (2024).
  - [2] “Standard test method for isothermal corrosion resistance of refractories to molten glass,” (2022).
  - [3] T. Jin, M. A. Hall, J. D. Vienna, W. C. Eaton, J. W. Amoroso, B. J. Wiersma, W. Li, A. W. Abboud, D. P. Guillen, and A. A. Kruger, International Materials Reviews 68 (2024), 10.1080/09506608.2023.2211469.
  - [4] P. J. Certa, R. Kirkbride, T. Hohl, P. Empey, M. Wells, et al., River Protection Project System Plan, Tech. Rep. (Hanford Site, Richland, WA (United States), 2009).
  - [5] J. D. Vienna, G. F. Piepel, D.-S. Kim, J. V. Crum, C. E. Lonergan, B. A. Stanfill, B. J. Riley, S. K. Cooley, and T. Jin, 2016 update of Hanford glass property models and constraints for use in estimating the glass mass to be produced at Hanford by implementing current enhanced glass formulation efforts, Tech. Rep. (Pacific Northwest National Lab.(PNNL), Richland, WA (United States), 2016).